Two-magnon inelastic light scattering in the antiferromagnets CoF_2 and NiF_2: Experiment and theory

E. Meloche,[1,*] M. G. Cottam,[1] and D. J. Lockwood[2]
[1]*Department of Physics and Astronomy, University of Western Ontario, London, Ontario, Canada, N6A 3K7*
[2]*Institute for Microstructural Sciences, National Research Council, Ottawa, Ontario, Canada, K1A 0R6*
(Received 23 September 2006; published 10 September 2007)

Experimental measurements for the two-magnon Raman scattering in the rutile-structure antiferromagnets CoF_2 and NiF_2 are reported. For CoF_2 the temperature and polarization dependences of the two-magnon scattering are investigated up to the Néel temperature T_N. An effective spin model is employed to obtain a good theoretical description of the line shapes and peak frequencies for temperatures up to $0.4T_N$. For NiF_2, we present results for the polarization characteristics of the scattering at low temperatures $T \ll T_N$. A theoretical model similar to that employed for CoF_2 is used to compare with the experimental measurements and good agreement is obtained for the line shapes and peak frequencies. Results are also deduced for some exchange and anisotropy parameters and the relative magnitudes of the magneto-optical coefficients in the interaction Hamiltonian for both CoF_2 and NiF_2.

DOI: 10.1103/PhysRevB.76.104406 PACS number(s): 72.10.Di, 78.20.Ls, 78.30.−j

I. INTRODUCTION

In this paper we present experimental and theoretical results for the two-magnon inelastic light scattering in the rutile-structure (space group $P4_2/mnm$ or D_{4h}^{14}) antiferromagnets CoF_2 (T_N=38 K) and NiF_2 (T_N=73 K). Other isomorphic compounds, including in particular FeF_2 and MnF_2, have been extensively studied because of the relative simplicity of the magnetic ordering and the theoretical results are in good agreement with experimental data over a broad range of temperatures.[1] Our Raman scattering data provide a systematic study of the polarization dependences for both CoF_2 and NiF_2 extending earlier measurements,[2–4] and necessitating the more detailed theoretical work presented here. Theories for the light scattering from magnon pairs have been developed by numerous authors, covering a wide range of temperatures (see Cottam and Lockwood[1] for a review). In this work we employ a Green's function theory similar to that used to analyze the two-magnon scattering spectrum in FeF_2 and MnF_2.[5] The formalism is extended here to CoF_2 and NiF_2 and detailed comparisons are made between the theory and the experimental measurements for the two-magnon line shapes and peak frequencies in various polarizations. Comparisons of theoretical and experimental integrated intensites in various polarizations enables us to deduce the relative values for the two-magnon magneto-optical coefficients appearing in the interaction Hamiltonian.

In the following section we describe the Raman experiments and present the results for the two-magnon scattering in the CoF_2 and NiF_2 samples. The theoretical analyses for the magnon excitations and the two-magnon scattering are described in Secs. III and IV, respectively, and comparisons of theory and experiment are presented in Sec. V. The conclusions of our work are given in Sec. VI.

II. EXPERIMENT AND RESULTS

The purplish-red-colored sample of CoF_2 was prepared from a single crystal grown at the Clarendon Laboratory, Oxford University, specially for this study. The cuboid sample of dimensions $3.2 \times 2.0 \times 1.7$ mm^3 was cut to expose (001) [Z], (110) [X], and (1$\bar{1}$0) [Y] faces, respectively, and these faces were highly polished with 1 μm diamond powder. The Raman spectrum was excited with 500 mW of Ti:sapphire laser light at 800 nm, which avoided any optical absorption,[6] analyzed with a Spex 14018 double monochromator at a spectral resolution of 4.1 cm^{-1}, and detected by a cooled RCA 31034A photomultiplier. The sample was mounted in the helium exchange-gas space of a Thor S500 continuous flow cryostat, where the temperature could be controlled to within 0.1 K and was measured with a gold-iron/chromel thermocouple clamped to the sample. Spectra were recorded in the 90° scattering geometry. The two-magnon scattering was measured in different polarizations for temperatures up to about T_N, but such scattering was found to be unimportant at higher temperatures, contrasting with the behavior observed for MnF_2, NiF_2, and FeF_2.[1]

In Fig. 1 we show the low-temperature Raman spectrum of CoF_2 recorded at frequencies up to 550 cm^{-1} in various polarizations. The spectra exhibit a number of features that can be associated either with vibrational or electronic excitations. Phonons of A_{1g}, B_{1g}, B_{2g}, and E_g symmetry are expected in the Raman spectrum of tetragonal CoF_2 and these are readily identified in our results following the work of Macfarlane and Ushioda.[7,8] Because of the 45° rotation of the crystal a and b axes with respect to the laboratory X and Y axes, respectively, the B_{2g} mode is no longer visible in $X(YX)Y$ polarization, but is seen for example in $Z(XX)Y$ polarization (not shown in Fig. 1). The other features shown in Fig. 1 all arise from electronic Raman scattering within Co^{2+} ions. The free-ion ^{4}F ground-state electronic energy levels give rise to a number of excitons in antiferromagnetically ordered CoF_2 at energies ranging up to 1400 cm^{-1} and many of these are Raman active.[8,9] On the basis of this earlier work, we have identified the excitons indicated by the labels Ex_i (i=1,...,4) in Fig. 1. The Ex_4 peak expected at 204 cm^{-1} in $X(YX)Y$ polarization was not seen in the earlier Raman study:[8] it is indeed quite weak. The lowest energy

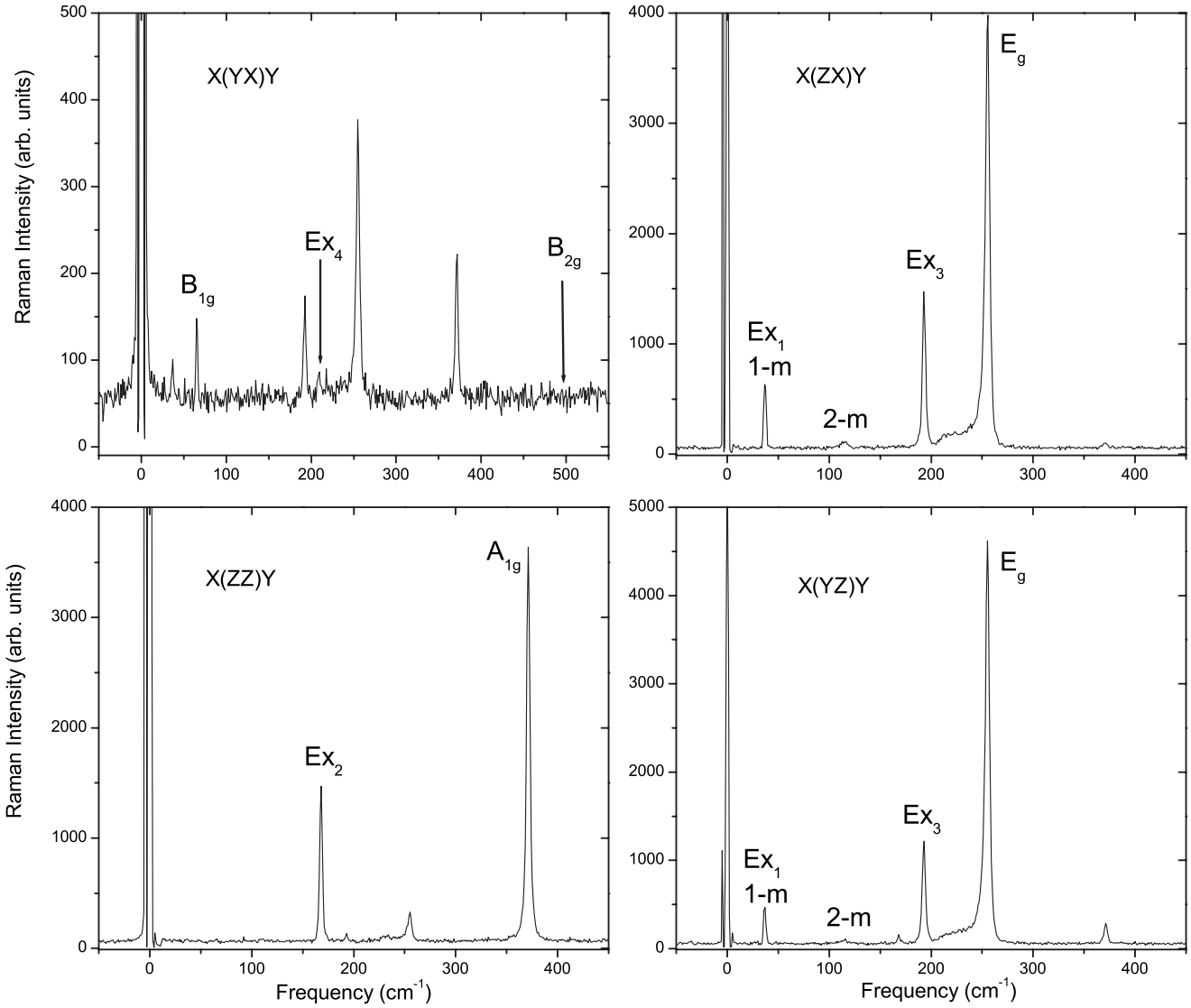

FIG. 1. Polarized Raman spectra of antiferromagnetic CoF_2 at 10 K showing features due to vibrational (A_{1g}, B_{1g}, and E_g) and electronic (Ex_1, Ex_2, Ex_3, and Ex_4) excitations. The B_{2g} phonon is absent in $X(YX)Y$ polarization consistent with the c axis rotation by 45° of the crystal a and b axes. The Ex_1 exciton feature corresponds to one-magnon (1-m) scattering. The two-magnon (2-m) scattering is seen to be comparatively weak.

exciton above the ground state is conventionally termed the one-magnon excitation. The two-magnon excitation in CoF_2 is seen from Fig. 1 to be much weaker than the exciton scattering, but, fortunately, it does not overlap with either the excitons or the phonons. Thus in the detailed polarization and temperature dependent studies reported next, the analysis of the two-magnon spectra is straightforward.

The temperature dependence of the strongest two-magnon Raman scattering in CoF_2 is shown for two representative polarizations in Figs. 2 and 3. Spectra in $X(YZ)Y$, $Y(ZX)Z$, and $Y(ZY)Z$ polarizations are all similar to those shown in Fig. 2. Weaker two-magnon features were observed in other polarizations (see Fig. 4). The two-magnon peaks near 110 cm^{-1} shown in Figs. 2 and 3 exhibit a similar symmetric line shape and integrated intensity at low temperature. With increasing temperature they both show shifts to lower frequency and increasing damping. However, there is one important difference, and that is the separation of 2.5 cm^{-1} between their peak frequencies at ~5 K. A similar separation (2.1 cm^{-1}) was reported earlier by Moch *et al.*,[10] but no spectra were given. In fact, to the best of our knowledge the only previously presented two-magnon spectrum for CoF_2 is that of Cipriani *et al.*[2] in (XZ) polarization. The weak scattering in $X(YX)Y$ polarization resembles that for $Y(XX)Z$ polarization shown in Fig. 3, while the scattering in $X(ZZ)Y$ polarization is broad and featureless.

The two-magnon bands were curve fitted with Gaussian-Lorentzian line shapes to extract their band parameters as a function of temperature. The results obtained for the peak frequencies, linewidths, and integrated intensities for the various polarizations at low temperatures are given in Table I. The corresponding temperature dependences are shown in Figs. 5–7, respectively, and are discussed in more detail later. We note that the intensity results shown in Fig. 7 confirm

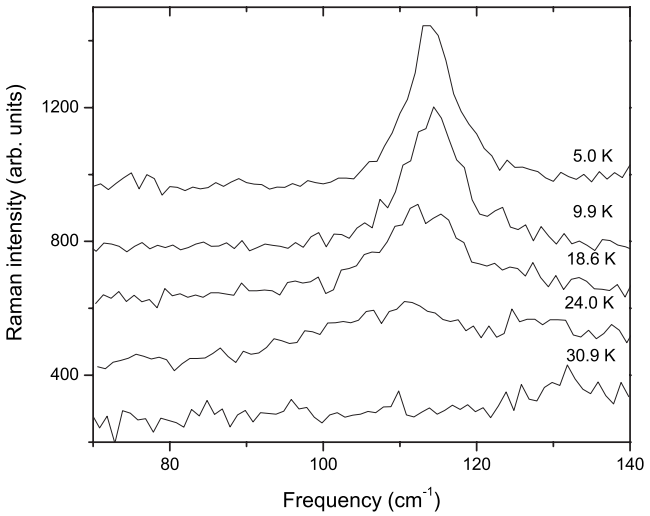

FIG. 2. Temperature dependence of the Stokes two-magnon Raman spectrum of CoF_2 in $X(ZX)Y$ polarization. The spectra are offset vertically for clarity.

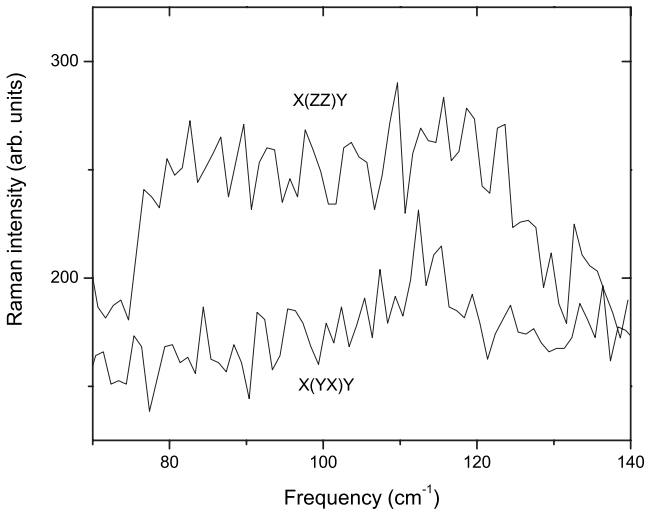

FIG. 4. Polarized Stokes Raman spectra of CoF_2 at low temperature (~5 K) in (ZZ) and (YX) polarizations. The spectra are offset for clarity.

what is partly evident in Figs. 2 and 3, namely the two-magnon scattering becomes unobservable at temperatures approaching T_N. This behavior is in sharp contrast with that observed for other rutile-structure antiferromagnets including MnF_2, NiF_2, and FeF_2,[1] where the two-magnon scattering persists as a heavily damped band to temperatures well above T_N. Hot-band Raman scattering is evident near 130 cm^{-1} in Figs. 2 and 3, respectively, due to thermal population of Co^{2+}-ion electronic states.

The yellowish-green-colored sample of NiF_2 was also fashioned from a single crystal obtained specially from Oxford University. Again, the sample was prepared in the form of a cuboid with (001) $[Z]$, (110) $[X]$, and $(1\bar{1}0)$ $[Y]$ faces and it had corresponding dimensions of $4.2\times3.7\times1.1$ mm^3. The Raman spectrum was excited with 300 mW of 514.5 nm argon ion laser light filtered by an Anaspec 300S prism monchromator. The use of green laser light minimized any sample heating due to optical absorption, especially at low temperatures. The rest of the experimental conditions were as for the CoF_2 sample, except that the spectrometer resolution was 1.9 cm^{-1}. Two-magnon Raman spectra were recorded in different polarizations at low temperatures only, as the temperature dependence of the two-magnon scattering has been investigated earlier by several authors.[1,3,11]

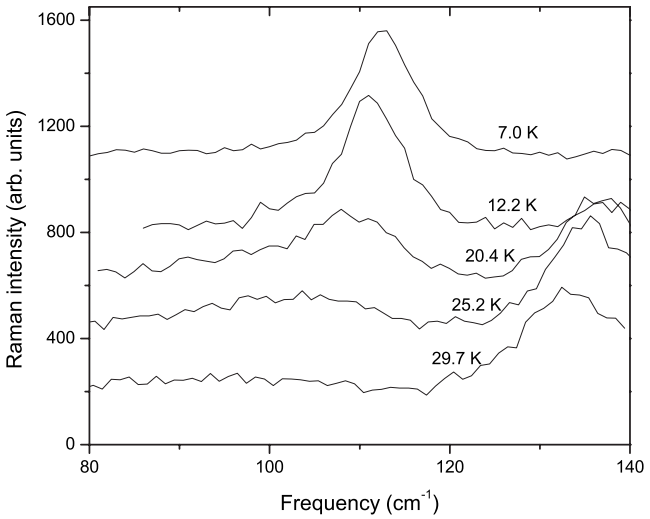

FIG. 3. As in Fig. 2 but in the $Y(XX)Z$ polarization.

The two-magnon Raman spectra obtained for NiF_2 at low temperatures are shown in Fig. 8. The strongest scattering occurred in $Z(XX)Y$ and $Z(YZ)Y=Z(XZ)Y=X(YZ)Y$ polarizations. The $X(ZX)Y$ spectrum was slightly (~10%) weaker than the three other (equivalent) spectra, due to a variation in the experimental conditions arising from a change in the sample optical transmission for this polarization. Apart from the factor of approximately 2 in peak intensity, the spectra for these two sets of two-magnon bands are apparently very similar. An earlier study performed on a sample with (100), (010), and (001) faces[3,4,11] indicated that the (XY), (XZ), and (YZ) spectra were practically identical with nearly symmetric line shapes and essentially the same peak intensity. From the spectra reported in Fig. 7 of Hutchings *et al.*,[4] we deduce that the integrated intensities of their (XY) and (XZ) polarized two-magnon spectra are in the ratio 1:0.8.

To obtain more precise information for the two-magnon band parameters for NiF_2, we have curve-fitted the spectra using a modified Gaussian line shape (the EMG model used by Lockwood and Wasilewski[12]) to take account of the noticeable asymmetry observed here in the two-magnon band line shape. Representative results for the fits are shown in Fig. 8. In general, the fits over most of the two-magnon line shape are excellent. The only problems occur in fitting the high-frequency tails of the strongest lines, where the model is an inadequate representation. Nevertheless, the results are good enough to give an accurate band frequency (the frequency at the band maximum) and linewidth, as well as a good indication of the integrated intensity (see Table II). The results indicate that, contrary to earlier work, there is a small

TABLE I. Band parameters of polarized Stokes two-magnon Raman scattering in CoF_2 at low temperatures ~5 K with the exception of ~10 K for the weak $X(YX)Z$ scattering. The standard errors from the fits are given in parentheses; FWHM is the band full-width at half-maximum. The integrated intensity is estimated from the area under the curves and scaled relative to the $Y(ZX)Z$ integrated intensity.

Polarization	Frequency (cm^{-1})	FWHM (cm^{-1})	Integrated intensity (arb. units)
$X(YX)Y$	111.65(1.24)	6.48(4.09)	0.086
$X(ZZ)Y$	99.26(1.22)	49.88(1.96)	0.327
$X(ZX)Y$	114.44(0.24)	7.64(0.12)	0.871
$X(YZ)Y$	114.05(0.30)	7.12(0.28)	0.871
$Y(XX)Z$	112.00(0.28)	7.48(0.24)	0.914
$Y(ZX)Z$	113.28(0.30)	7.98(0.35)	1.000
$Y(ZY)Z$	113.75(0.30)	7.46(0.30)	0.839

but discernable difference (0.4 cm^{-1} on average) between the band frequencies in $Z(XX)Y$ and $Z(YZ)Y=Z(XZ)Y=X(YZ)Y=X(YZ)Y$ polarizations. These results together with those obtained for the weaker bands in $X(YX)Y$ and $X(ZZ)Y$ polarizations shown in Fig. 8 will be discussed in Sec. IV.

III. THEORY OF MAGNON EXCITATIONS

A. CoF_2

We represent CoF_2 using the following effective spin $S=1/2$ Hamiltonian:

$$H=\sum_{i,j}J_{i,j}\mathbf{S}_i\cdot\mathbf{S}_j+\frac{1}{2}\sum_{i,i'}J'_{i,i'}\mathbf{S}_i\cdot\mathbf{S}_{i'}+\frac{1}{2}\sum_{j,j'}J'_{j,j'}\mathbf{S}_i\cdot\mathbf{S}_{j'}-H_A(T)\times\left(\sum_i S_i^z-\sum_j S_j^z\right),\quad(1)$$

where $J_{i,j}$ represents the dominant antiferromagnetic exchange between sites on different sublattice whereas $J'_{i,i'}$ and $J'_{j,j'}$ are the intrasublattice exchanges. The effective anisotropy field $H_A(T)$ is assumed to vary with temperature like the sublattice magnetization and is written as $H_A(T)=H_A(0)\times\langle S^z\rangle/S$. The parameters for the $S=1/2$ model have previously been estimated by comparing theory with one-magnon inelastic neutron scattering measurements[13] and the results are $J_1=-2.0$ cm^{-1}, $J_2=12.3$ cm^{-1}, $J_3\sim 0$ cm^{-1}, and $H_A(0)=12.5$ cm^{-1} where the exchange parameters are defined in Fig. 9.

The linearized magnon energies obtained from the Hamiltonian (1) are written as

$$E(\mathbf{k})=\sqrt{\mu^2(\mathbf{k})-[\langle S^z\rangle J_2(\mathbf{k})]^2},\quad(2)$$

where $\mathbf{k}$ is the wave vector and we have defined

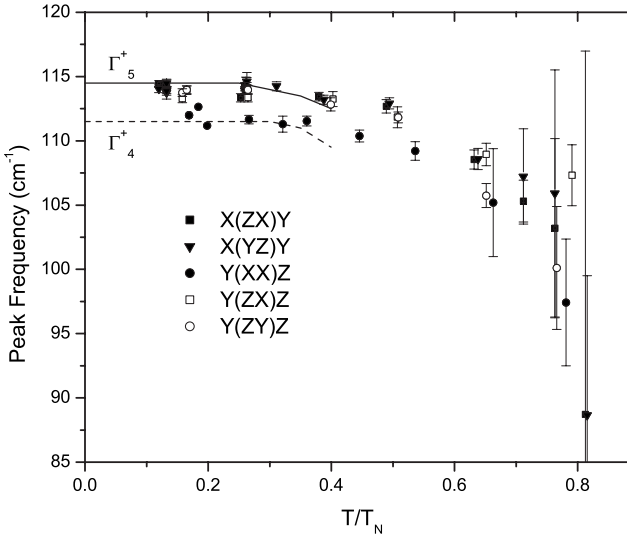

FIG. 5. Temperature dependence of the two-magnon peak frequency in CoF_2 for various polarizations. The dashed and solid lines represent the calculated peak frequency of the Γ_4^+ and Γ_5^+ modes, respectively.

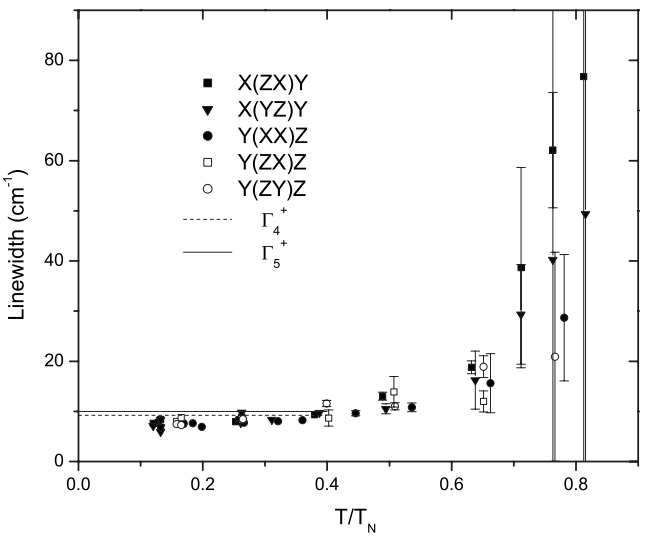

FIG. 6. Temperature dependence of the two-magnon linewidth (full-width at half-maximum) in CoF_2 for various polarizations. The dashed and solid lines represent the calculated linewidth of the Γ_4^+ and Γ_5^+ modes, respectively, at low temperatures.

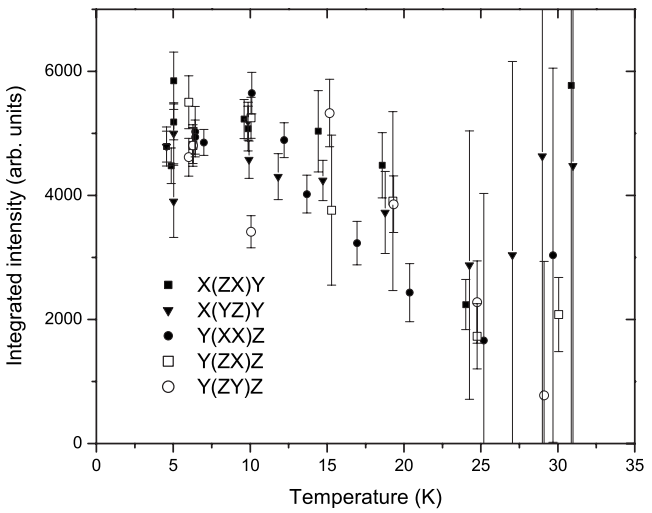

FIG. 7. Temperature dependence of the two-magnon integrated intensity in CoF_2 for various polarizations.

$$\mu(\mathbf{k}) = H_A(T) + 8\langle S^z\rangle J_2 - 4\langle S^z\rangle J_1 \sin^2(k_z c/2) - 4\langle S^z\rangle J_3[\sin^2(k_x a/2) + \sin^2(k_y a/2)],$$

$$J_2(\mathbf{k}) = 8J_2 \cos(k_x a/2)\cos(k_y a/2)\cos(k_z c/2). \quad (3)$$

For the numerical calculations to be presented in Sec. V the sublattice magnetization $\langle S^z\rangle$ is evaluated using a mean-field approximation.

B. NiF_2

We represent NiF_2 using the following spin $S=1$ Hamiltonian,

$$H = \sum_{i,j} J_{i,j}\boldsymbol{S}_i\cdot\boldsymbol{S}_j + \frac{1}{2}\sum_{i,i'} J'_{i,i'}\boldsymbol{S}_i\cdot\boldsymbol{S}_{i'} + \frac{1}{2}\sum_{j,j'} J'_{j,j'}\boldsymbol{S}_j\cdot\boldsymbol{S}_{j'} + \sum_i \{D(S_i^z)^2 - F[(S_i^x)^2 - (S_i^y)^2]\} + \sum_j \{D(S_j^z)^2 + F[(S_j^x)^2 - (S_j^y)^2]\}, \quad (4)$$

where the exchange interactions are defined as for CoF_2. A more precise representation is required here for the anisotropy using parameters D and F, which describe the effects of the uniaxial and nonuniaxial contributions to the single-ion anisotropy, respectively. Approximate values of the parameters have been previously determined by comparing theory with inelastic light scattering measurements and inelastic neutron scattering measurements[4] and are $J_1 = -0.22\pm0.5$ cm^{-1}, $J_2 = 13.87\pm0.36$ cm^{-1}, $J_3 = 0.79\pm0.40$ cm^{-1}, $D = 4.36\pm0.14$ cm^{-1}, and $F = 1.66\pm0.03$ cm^{-1}.

The anisotropy in NiF_2 causes the spins to lie in the plane perpendicular to the c axis (rather than parallel as in CoF_2) and to be canted slightly in the a-b plane away from the antiparallel alignment. The low-temperature canting angle has been estimated by several authors[1,4] and its value is approximately 0.5°. The spin canting in NiF_2 gives rise to a weak ferromagnetic moment which modifies the magnetic properties from those of isomorphic compounds such as MnF_2, FeF_2, and CoF_2, where the spin canting is absent. More specifically, it leads to an additional (lower-energy) branch in the magnon spectrum. The zone-center ($\mathbf{k}=0$) energy of the lower branch (at 3.3 cm^{-1}) is extremely sensitive to the choice of the nonuniaxial parameter F. By contrast, the nonuniaxial anisotropy has negligible effect on the zone-edge excitations in NiF_2. We have recently reported briefly on some properties of the one-magnon Raman light scattering in NiF_2,[16] and a more detailed account will be presented elsewhere. For the purposes of the two-magnon scattering, which is strongly weighted by zone-edge magnons,[1,3] we are justified in neglecting the contributions from the nonuniaxial anisotropy (i.e., we set $F=0$). In the low-temperature limit the magnon energies for NiF_2 are then written as

$$E_1(\mathbf{k}) = \sqrt{\mu^2(\mathbf{k}) - [SJ_2(\mathbf{k}) - SD/2]^2},$$

$$E_2(\mathbf{k}) = \sqrt{\mu^2(\mathbf{k}) - [SJ_2(\mathbf{k}) + SD/2]^2}, \quad (5)$$

where $\mu(\mathbf{k})$ is defined as in Eq. (3) for CoF_2 but with the replacements $\langle S^z\rangle \to S$ and $H_A(0) \to SD/2$. The higher-energy mode in NiF_2 with energy $E_1(\mathbf{k})$ is similar to the magnon branch obtained for CoF_2 in Eq. (2). Thus, for the purposes of the two-magnon scattering, we shall represent NiF_2 as a simple two-sublattice antiferromagnet with a dispersion relation given by $E_1(\mathbf{k})$. This simplified model neglects the canting of the spins in the a-b plane and so does not predict the correct energy gap for the $\mathbf{k}=0$ lower-energy magnon branch $E_2(0)$ but is an excellent approximation for the zone-edge magnons probed in two-magnon light scattering experiments. This approximation is expected to be less accurate for the two-magnon Γ_1^+ mode (see Sec. IV) which is more strongly influenced by magnons near the zone center. However, the Γ_1^+ mode typically appears as a flat nonresonant band and is less dependent on the model parameters.

IV. ANALYSIS OF THE TWO-MAGNON SPECTRUM

The Hamiltonian describing the interaction of light with a rutile-structure antiferromagnet may be written as[1,14]

$$H_{\text{int}} = \frac{1}{2}\sum_{\mathbf{r},\boldsymbol{\delta}} \phi(\boldsymbol{\delta})(S_{\mathbf{r}}^+ S_{\mathbf{r}+\boldsymbol{\delta}}^- + S_{\mathbf{r}}^- S_{\mathbf{r}+\boldsymbol{\delta}}^+ + \gamma S_{\mathbf{r}}^z S_{\mathbf{r}+\boldsymbol{\delta}}^z), \quad (6)$$

where $\mathbf{r}$ is summed over all the magnetic sites in the crystal, $\boldsymbol{\delta}$ is a vector connecting a magnetic site with one of its next-nearest neighbors (i.e., on the opposite sublattice), and γ is a weighting factor. The symmetry factor $\phi(\boldsymbol{\delta})$ may be written as

$$\phi(\boldsymbol{\delta}) = \{B_1(e_I^x e_S^x + e_I^y e_S^y) + B_2 e_I^z e_S^z + B_3(e_I^x e_S^y + e_I^y e_S^x)\sigma_{\boldsymbol{\delta}}^x\sigma_{\boldsymbol{\delta}}^y + B_4[(e_I^x e_S^z + e_I^z e_S^x)\sigma_{\boldsymbol{\delta}}^x\sigma_{\boldsymbol{\delta}}^z + (e_I^y e_S^z + e_I^z e_S^y)\sigma_{\boldsymbol{\delta}}^y\sigma_{\boldsymbol{\delta}}^z] + B_5[(e_I^x e_S^z - e_I^z e_S^x)\sigma_{\boldsymbol{\delta}}^x\sigma_{\boldsymbol{\delta}}^z + (e_I^y e_S^z - e_I^z e_S^y)\sigma_{\boldsymbol{\delta}}^y\sigma_{\boldsymbol{\delta}}^z]\}, \quad (7)$$

where $B_n (n=1,\ldots,5)$ are the magneto-optical coupling coefficients and $\sigma_{\boldsymbol{\delta}}^\alpha = \text{sign}(\boldsymbol{\delta}^\alpha)$ for $\alpha = x,y,z$. The polarizations are written with respect to the crystal axes (x,y,z) defined as in Fig. 9. The various magneto-optical coupling coefficients

(or combinations of coefficients) may be measured by varying the experimental polarizations of the incident and scattered light. Contributions from the antisymmetric polarizations terms in Eq. (7) have been shown experimentally to be negligible for MnF_2 and FeF_2.[5] An additional contribution to H_{int} which is allowed by symmetry but usually neglected is

$$\frac{1}{2}\sum_{\mathbf{r},\boldsymbol{\delta}} \phi'(\boldsymbol{\delta})(S^+_{\mathbf{r}}S^-_{\mathbf{r}+\boldsymbol{\delta}} - S^-_{\mathbf{r}}S^+_{\mathbf{r}+\boldsymbol{\delta}}), \tag{8}$$

where

$$\phi'(\boldsymbol{\delta}) = i[B_6(e^x_I e^x_S - e^y_I e^y_S) + B_7(e^x_I e^y_S - e^y_I e^x_S)\sigma^x_{\boldsymbol{\delta}}\sigma^y_{\boldsymbol{\delta}}], \tag{9}$$

and B_6 and B_7 are additional magneto-optical coupling coefficients. Interaction terms involving antisymmetric spin combinations, like in Eq. (8), may be important in effective spin systems like CoF_2 where the large effective anisotropy field is attributed to an unquenched orbital motion.[14]

The two-magnon line shapes, peak frequencies, and integrated intensities for different polarizations are analyzed using a similar temperature-dependent Green function theory to that in Ref. 5. The two-magnon scattering intensity (including magnon-magnon interactions) as a function of the energy shift E is proportional to

$$\frac{d^2h}{d\Omega d\omega_S} \propto \frac{\langle S^z\rangle^2\mu(0)}{1-\exp(-\beta E)}\,\mathrm{Im}\left(\frac{G_0(E)}{1+tG_0(E)}\right), \tag{10}$$

where $\mu(0)$ is defined in Eq. (3) and the quantities t and $G_0(E)$ depend on the polarizations. The noninteracting Green function represented by $G_0(E)$ may be written as

$$G_0(E) = \frac{1}{N}\sum_{\mathbf{k}} \frac{\mu(\mathbf{k})\Phi(\mathbf{k})\coth[\beta E(\mathbf{k})/2]}{E(\mathbf{k})[E-2E(\mathbf{k})+i2\Gamma(\mathbf{k})][E+2E(\mathbf{k})+i2\Gamma(\mathbf{k})]}. \tag{11}$$

Here N is the number of magnetic sites in each sublattice,

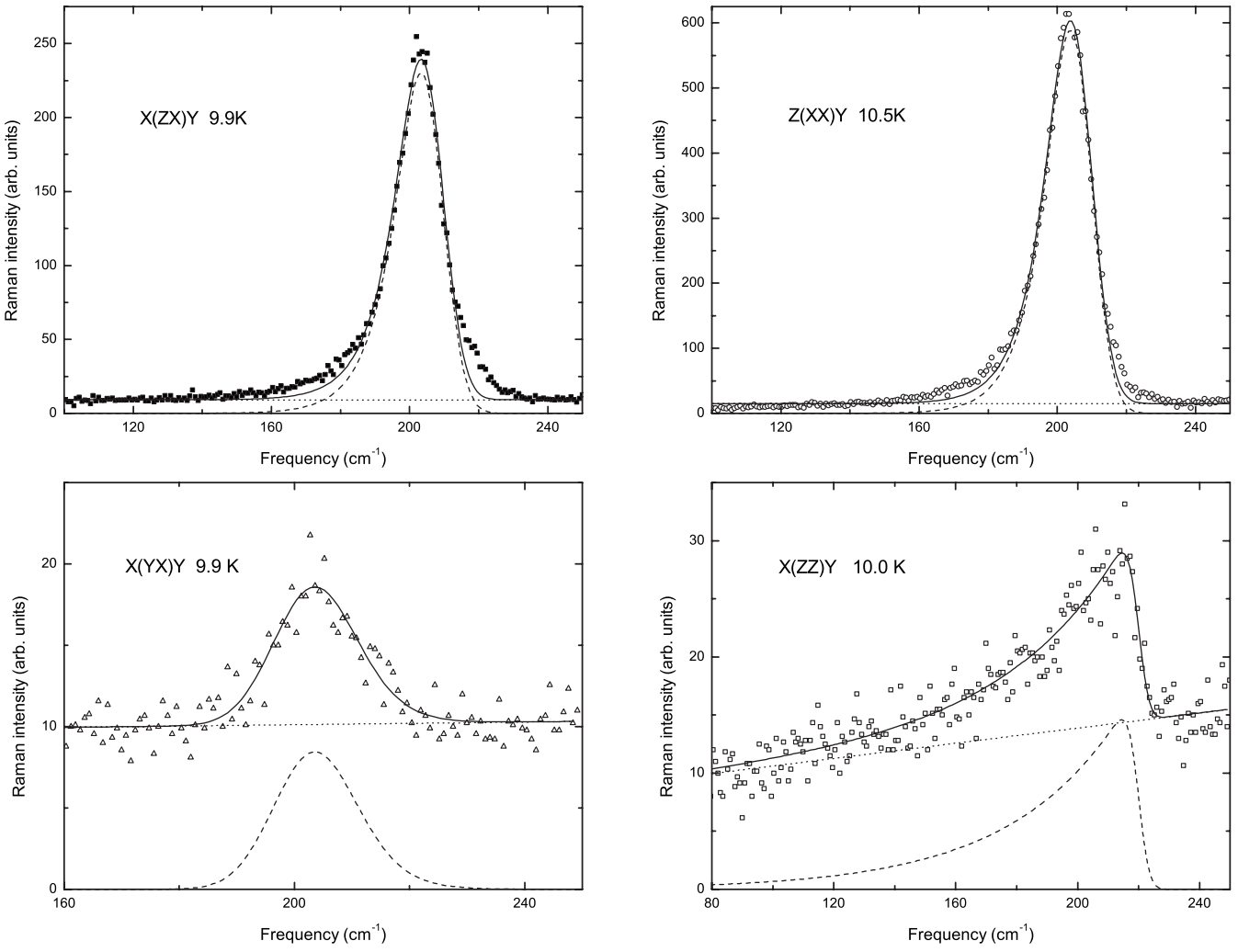

FIG. 8. Low-temperature two-magnon Raman Stokes scattering in NiF_2 recorded in four different polarizations. The observed line shapes have been fitted to obtain the two-magnon band parameters of frequency, linewidth, and integrated intensity. The fits are shown by the solid lines passing through the experimental points and the fitted bands (dashed lines) with background subtracted are shown below the experimental data.

TABLE II. Band parameters of polarized Stokes two-magnon Raman scattering in NiF_2 at ~10 K obtained by curve resolving. The standard errors from the fits are given in parentheses; FWHM is the band full-width at half-maximum. The integrated intensity is estimated from the area under the curves and scaled relative to the $Z(YZ)Y$ integrated intensity.

Polarization	Frequency (cm^{-1})	FWHM (cm^{-1})	Integrated intensity (arb. units)
$X(YX)Y$	203.54(1.53)	17.16(2.00)	0.026
$X(ZZ)Y$	214.54(0.31)	32.49(4.81)	0.105
$X(YZ)Y$	203.19(0.12)	16.43(0.33)	0.987
$X(ZX)Y$	203.37(0.12)	16.56(0.34)	0.873
$Z(XX)Y$	203.79(0.08)	16.06(0.24)	2.058
$Z(XZ)Y$	203.28(0.12)	16.74(0.31)	0.989
$Z(YZ)Y$	203.48(0.13)	16.91(0.36)	1.000
$Z(YX)Y$	204.32(0.36)	16.97(0.98)	0.085
$Z(XX)Y$	203.64(0.10)	16.15(0.27)	1.946
$Z(YX)Y$	203.09(0.85)	15.89(1.37)	0.045

$\Gamma(\mathbf{k})$ represents the effective one-magnon damping term, and $\Phi(\mathbf{k})$ is a symmetry weighting factor for each Raman active mode given by

$$\Phi(\mathbf{k}) = \begin{cases} 8\cos^2(k_x a/2)\cos^2(k_y a/2)\cos^2(k_z c/2) & \text{for } \Gamma_1^+, \\ 8\sin^2(k_x a/2)\sin^2(k_y a/2)\cos^2(k_z c/2) & \text{for } \Gamma_4^+, \\ 8\cos^2(k_x a/2)\sin^2(k_y a/2)\sin^2(k_z c/2) & \text{for } \Gamma_5^+. \end{cases} \tag{12}$$

The parameter t in Eq. (10) is due to the magnon interaction effects and in the limit of small intrasublattice exchange $J_2 \gg |J_1|$ and $J_2 \gg |J_3|$, appropriate for both CoF_2 and NiF_2, the parameter is approximately given by

$$t = \begin{cases} 4J_2[\mu(0) - 4\langle S^z\rangle J_2] & \text{for } \Gamma_1^+, \\ 4J_2\mu(0) & \text{for } \Gamma_4^+ \text{ and } \Gamma_5^+. \end{cases} \tag{13}$$

The symmetry weighting factors defined in Eq. (12) emphasize different points in the Brillouin zone. The difference in magnon frequency between the R point, at $\mathbf{k}=(0,\pi/a,\pi/c)$, and M point, at $\mathbf{k}=(\pi/a,\pi/a,0)$, is

$$E(R) - E(M) = 4\langle S^z\rangle(J_3 - J_1), \tag{14}$$

and so the splitting of the two-magnon peak frequency between the Γ_4^+ and Γ_5^+ modes is expected to be of the order $8\langle S^z\rangle(J_3 - J_1)$.

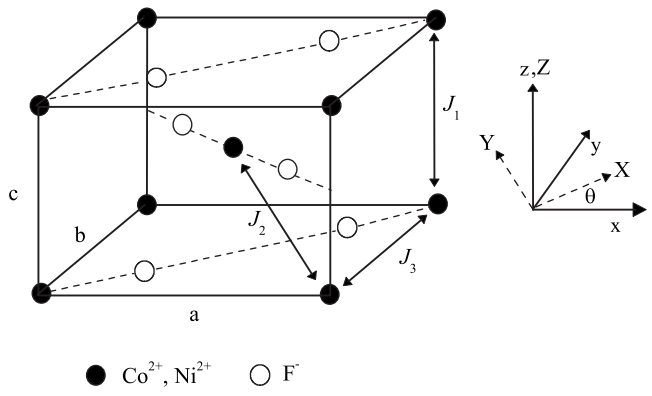

FIG. 9. The crystallographic unit cell of CoF_2 and NiF_2 with the dominant exchange interactions marked. The crystal axes (x,y,z) and laboratory axes (X,Y,Z) are illustrated in relation to the unit cell.

The effective one-magnon damping term $\Gamma(\mathbf{k})$ in Eq. (11) typically includes contributions from four-magnon scattering processes and the scattering of magnons by longitudinal spin fluctuations which are temperature and wave-vector dependent. Recent one-magnon lifetime measurements using a neutron spin-echo method[15] on the antiferromagnet MnF_2 are in good agreement with the theory based on longitudinal spin fluctuations over a wide range of temperatures and wave vectors. However, due to the lack of high-resolution experimental data on CoF_2 and NiF_2 it is difficult to determine the intrisic magnon lifetimes throughout the Brillouin zone. The effective damping in our theory should also include a nonintrinsic contribution to represent the instrumental resolution. For simplicity we set the damping $\Gamma(\mathbf{k})$ equal to the resolution half-width (defined as Γ) in the one-magnon scattering experiments.

Experimentally, the Γ_1^+ mode may be investigated by means of the diagonal polarizations (xx), (yy), and (zz), the Γ_4^+ modes by (xy) or (yx) polarizations, and the Γ_5^+ modes by (xz), (zx), (yz), and (zy) polarizations. In writing Eq. (10) we have omitted the modulus squared of the magneto-optical coefficients which come in as an overall multiplicative proportionality factor. For example, the scattering intensity in the diagonal polarization (xx) is also proportional to $|B_1|^2$ whereas in the off-diagonal polarization (xy) it is proportional to $|B_3|^2$.

When the polarizations of the incident and scattered electric fields are written with respect to a coordinate system that is rotated about the c (Z) axis through an angle θ the symmetry weighting factor defined in Eq. (7) may be written as

$$\phi(\boldsymbol{\delta}) = [B_1 + B_3 \sin(2\theta)\sigma^x_{\boldsymbol{\delta}}\sigma^y_{\boldsymbol{\delta}}](e^X_I e^X_S + e^Y_I e^Y_S) + B_2 e^Z_I e^Z_S + B_3 \cos(2\theta)\sigma^x_{\boldsymbol{\delta}}\sigma^y_{\boldsymbol{\delta}}(e^X_I e^Y_S + e^Y_I e^X_S) + (B_4 + B_5) \times [(\sin\theta\sigma^y_{\boldsymbol{\delta}}\sigma^z_{\boldsymbol{\delta}} + \cos\theta\sigma^x_{\boldsymbol{\delta}}\sigma^z_{\boldsymbol{\delta}})e^X_I e^Z_S + (\cos\theta\sigma^y_{\boldsymbol{\delta}}\sigma^z_{\boldsymbol{\delta}} - \sin\theta\sigma^x_{\boldsymbol{\delta}}\sigma^z_{\boldsymbol{\delta}})e^Y_I e^Z_S] + (B_4 - B_5)[(\sin\theta\sigma^y_{\boldsymbol{\delta}}\sigma^z_{\boldsymbol{\delta}} + \cos\theta\sigma^x_{\boldsymbol{\delta}}\sigma^z_{\boldsymbol{\delta}})e^Z_I e^X_S + (\cos\theta\sigma^y_{\boldsymbol{\delta}}\sigma^z_{\boldsymbol{\delta}} - \sin\theta\sigma^x_{\boldsymbol{\delta}}\sigma^z_{\boldsymbol{\delta}})e^Z_I e^Y_S]. \quad (15)$$

The experimental spectra recorded in the (XX) polarization will represent a mixture of the Γ_1^+ and Γ_4^+ Raman active modes which are proportional to $|B_1|^2$ and $|B_3 \sin(2\theta)|^2$, respectively. The mixing of the Γ_1^+ and Γ_4^+ modes also produces a cross term proportional to $B_1 B_3 \sin(2\theta)$. However, this latter term will eventually cancel out on numerical integration over the Brillouin zone.

V. COMPARISON BETWEEN THEORY AND EXPERIMENT

A. CoF_2

Using the parameters from Ref. 10, the two-magnon peak frequency in CoF_2 for the Γ_5^+ mode is expected to be greater than the Γ_4^+ mode and the predicted splitting of the peaks in the low-temperature limit should be approximately 8 cm^{-1}. Our Raman data indicates that the splitting of the two-magnon peaks in the low-temperature limit is actually $\sim$2.5 cm^{-1} suggesting that the difference between the intrasublattice exchanges J_3 and J_1 should be less than that implied by the neutron scattering data. To compare the low-temperature theoretical and experimental results we set the damping term equal to the resolution half-width in the experiments (i.e., we set $\Gamma = 2.05$ cm^{-1}). In principle the damping term can also include a contribution from the intrinsic one-magnon damping at the zone boundary. The summation over the Brillouin zone in Eq. (11) is evaluated in terms of a numerical integration.

The numerical calculations for CoF_2 are made using $J_1 = -1.2$ cm^{-1}, $J_2 = 12.9$ cm^{-1}, $J_3 \sim 0$ cm^{-1}, and $H_A(0) = 12.0$ cm^{-1} as our optimal set of parameters. We obtain these parameter values by comparing theory with experiment for the zone-center one-magnon frequency $\sim$37 cm^{-1}, as well as the two-magnon line shapes and peak frequencies for the Γ_4^+ and Γ_5^+ modes. While the behavior of the line shapes and peak frequencies of the two-magnon scattering for the Γ_4^+ and Γ_5^+ modes is sensitive to the choice of exchange and anisotropy parameters, the weaker Γ_1^+ scattering gives rise to a broad featureless line shape because of the weighting of the zone-center point and is less dependent on the model parameters. Here the diagonal polarization (XX) does not appear as a flat nonresonant band because of the 45° rotation of the experimental X and Y axes with respect to the crystallographic a and b axes. When the symmetry factor $\phi(\boldsymbol{\delta})$ is written with respect to the laboratory coordinate system, the (XX) experimental polarization actually represents a mixture of the Γ_1^+ and Γ_4^+ Raman active modes.

In Fig. 10(a) we compare theory and experiment for the low-temperature ($T \sim 5$ K) two-magnon Raman intensities in (XX) polarization. By comparing theory with experiment for the intergrated intensites in (XX) polarization we are able to estimate the relative magnitudes of the magneto-optical coefficients B_1 and B_3. The theory curve is obtained using $|B_1| = 0.2|B_3|$ which represents an upper limit for the magnitude of B_1 relative to B_3. The small contribution of the Γ_1^+ mode does not shift the peak frequency and its main effect is to increase the height of the tail of the peak at lower frequencies. The mixing of the Γ_1^+ and Γ_4^+ modes also leads to cross terms proportional to $B_1 B_3 \sin(2\theta)$. However, these terms cancel out on numerical integration over the Brillouin zone.

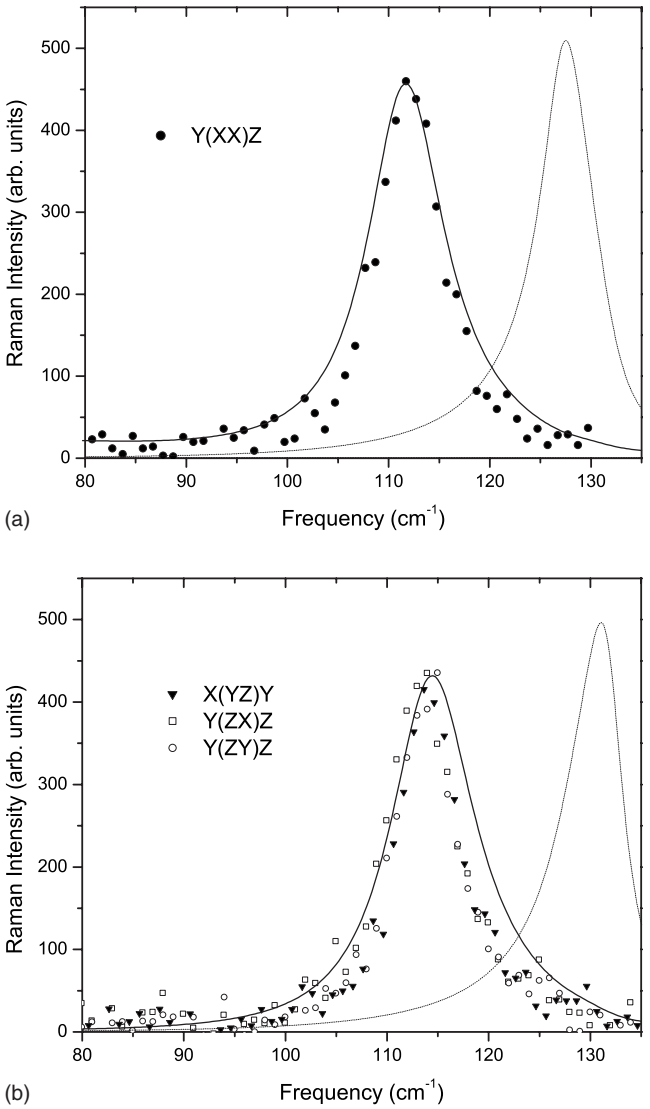

FIG. 10. Comparison of theory curve and experimental points for the low-temperature two-magnon Raman spectrum of CoF_2 in (a) diagonal and (b) off-diagonal polarizations. The dotted lines show the results without the inclusion of magnon-magnon interactions.

In Fig. 10(b) we compare theory with experiment for the off-diagonal polarizations $X(ZX)Z$, $Y(ZX)Z$, and $Y(ZY)Z$, all of which represent the Γ_5^+ mode only. The rotation to the laboratory coordinate system does not produce any mixing effects because the crystal c axis coincides with the laboratory Z axis. The main effect of the rotation of the laboratory

axes with respect to the crystal axes is to produce symmetric and antisymmetric combinations of the B_4 and B_5 magneto-optical coupling coefficients. The two-magnon scattering intensity is proportional to $|B_4+B_5|^2$ for the (XZ) and (YZ) polarizations and to $|B_4-B_5|^2$ for the (ZX) and (ZY) polarizations. These terms represent overall multiplicative factors that do not affect the line shapes of the spectra. The experimental spectra are effectively identical in all of these polarizations and thus we are unable to deduce the relative values of B_4 and B_5 for CoF_2 except to conclude that one of these must be far greater in magnitude than the other. By comparing the integrated intensities in Figs. 10(a) and 10(b) we are able to deduce that $|B_4 \pm B_5| \sim 0.7|B_3|$. Also, making use of the data in (ZZ) polarization, we are able to deduce that $|B_2|/|B_3| \simeq 0.6$.

The experimental spectrum in the (YX) polarization (see Fig. 4) reveals a two-magnon peak frequency at 113 ± 1 cm^{-1} and an integrated intensity that is $\sim 10\%$ of the integrated intensity in other off-diagonal polarizations. The terms involving the (YX) polarization in Eq. (8) vanish for a rotation through an angle of 45°, and thus the intensity for this polarization [as well as the (XY) polarization] is expected to be much weaker than in other off-diagonal polarizations. The origin of the two-magnon feature in the (YX) polarization may be attributed to a small misalignment of the axes and/or to the additional interaction term in Eq. (8) which involves different combinations of the incident and scattered polarizations. When $\phi'(\boldsymbol{\delta})$ is rewritten with respect to the laboratory coordinate system the scattering intensity will depend on the additional magneto-optical coefficients B_6 and B_7. By comparing theory with experiment we are able to estimate the relative values of the magneto-optical coefficients and we find $|B_6| \sim 0.3|B_7|$.

In Figs. 5 and 6 for CoF_2 we compare the temperature dependences of the two-magnon peak frequencies and linewidth, respectively, in various polarizations. The theoretical results obtained from the simplified spin $S=1/2$ model are found to be in good agreement with experimental data for temperatures up to $T \sim 0.4\ T_N$.

B. NiF_2

In Fig. 11(a) we compare theory with experiment for the (XX) diagonal polarization. The solid line represents the Γ_4^+ mode only and is obtained using $J_1=0.2$ cm^{-1}, $J_2=13.8$ cm^{-1}, $J_3=0.3$ cm^{-1}, $D=4.2$ cm^{-1} which represents our optimal set of parameters for NiF_2. The theory curves for NiF_2 are obtained with the damping $\Gamma=0.95$ cm^{-1}. The dotted line represents the theory curve without the inclusion of magnon-magnon interactions. The theoretical two-magnon peak frequencies for the Γ_4^+ and Γ_5^+ modes are 203.3 cm^{-1} and 203.7 cm^{-1}, respectively. For comparison, the dashed line shows the predicted two-magnon intensity using the set of parameters of Ref. 4. Here the height of the spectrum is scaled to coincide with the experimental maximum intensity. Although the theory predicts some mixing of the Γ_1^+ and Γ_4^+ modes in this polarization we obtain a very good fit to the experimental data without any admixture of the Γ_1^+ mode, implying that the magnitude of the magneto-optical coefficient $|B_1| \ll |B_3|$.

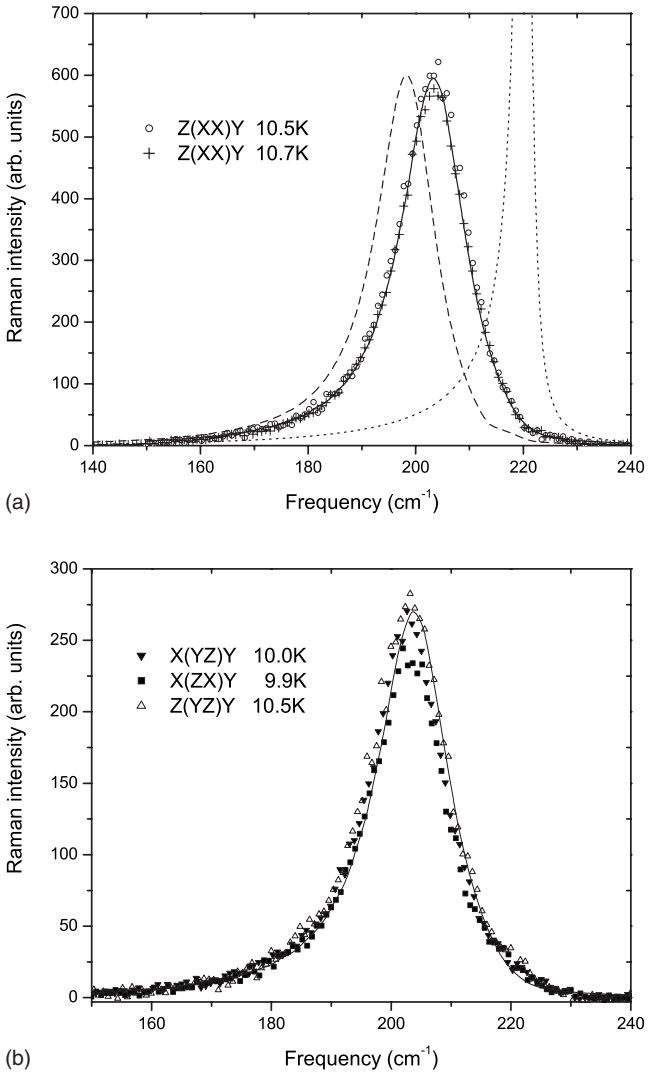

FIG. 11. Comparison of theory curves (see text) and experimental points for the low-temperature two-magnon Raman spectrum of NiF_2 in various polarizations.

In Fig. 11(b) we compare theory with experiment for the off-diagonal polarizations $X(YZ)Y$, $X(ZX)Y$, and $Z(YZ)Y$. All of these experimental polarizations investigate the Γ_5^+ mode only. As in CoF_2, the experimental spectra in these polarizations have similar line shapes and integrated intensities and thus we are unable to deduce relative values of the magneto-optical coefficients B_4 and B_5 except to conclude that one is far greater in magnitude than the other. By comparing the integrated intensities in the different off-diagonal polarizations we find that $|B_4 \pm B_5| \sim 0.5|B_3|$.

The weaker scattering in the (YX) polarization may be attributed to the 45° rotation of the experimental axes with respect to the crystal axes. Allowing for the possibility of a small misalignment of the axes we expect a weak scattering signal with the spectral features of the Γ_4^+ mode. The weak scattering spectrum in the diagonal polarization (ZZ) gives an asymmetric line shape (see Fig. 8) with a peak frequency

that is $\sim 10\ \mathrm{cm}^{-1}$ greater than the peak frequencies observed in other polarizations. A similar feature was observed for the two-magnon spectrum in the (ZZ) polarization in FeF_2.[17] The calculated spectrum for the (ZZ) polarization appears as a flat nonresonant band because of weighting of the zone-center point and does not account well for the peak feature observed in the experimental measurement. Nevertheless, from the integrated intensity we deduce that $|B_2|/|B_3| \simeq 0.2$.

VI. CONCLUSION

In summary we have presented experimental results to investigate the temperature and polarization dependences for two-magnon Raman scattering in the rutile-structure antiferromagnets CoF_2 and NiF_2. Our theoretical analysis has allowed us to deduce the dominant exchange and anisotropy parameters more accurately and to determine the relative values for some of the magneto-optical coupling coefficients in the interaction Hamiltonian.

For CoF_2, the present theory gives good agreement for the two-magnon peak frequencies and linewidths for temperatures up to 0.4 T_N but does not hold for higher temperatures due to the complexity of this material. At higher temperatures, a generalized theory of CoF_2 that incorporates additional magnon interaction terms and/or the effects of the orbital angular momentum (necessitating an effective $S=3/2$ model[18]) is required. For CoF_2 our optimal set of exchange and anisotropy parameters are $J_1=-1.2\ \mathrm{cm}^{-1}$, $J_2=12.9\ \mathrm{cm}^{-1}$, $J_3 \sim 0\ \mathrm{cm}^{-1}$, and $H_A(0)=12.0\ \mathrm{cm}^{-1}$. These are similar to the previously determined values obtained by comparing theory with one-magnon inelastic neutron scattering measurements.[13] However, some adjustments of the parameter values were made to properly account for the difference in the two-magnon peak frequency between the Γ_4^+ and Γ_5^+ Raman modes. By comparing the integrated intensites of the two-magnon spectra in various experimental polarizations we are able to determine the *relative* magnitudes for some of the magneto-optical coefficients defined in Eqs. (7) and (9), as discussed earlier.

TABLE III. Comparison of the relative values of several dominant magneto-optical coupling coefficients for two-magnon Raman scattering in rutile-structure MF_2 antiferromagnets (with M=Co, Ni, Mn, and Fe). The MnF_2 and FeF_2 data are taken from Ref. 5; $|B_5| \ll |B_4|$ for both of these compounds.

Compound	$\lvert B_1\rvert/\lvert B_3\rvert$	$\lvert B_2\rvert/\lvert B_3\rvert$	$\lvert B_4 \pm B_5\rvert/\lvert B_3\rvert$
CoF_2	0.2	0.6	0.7
NiF_2	~ 0	0.2	0.5
MnF_2	0.14	0.32	0.66
FeF_2		0.3	0.8

For NiF_2 we have presented results regarding the polarization dependence of the low-temperature two-magnon Raman scattering, extending earlier works done by Fleury[3] and Hutchings *et al.*[4] The theoretical model includes the effects of the three dominant exchange parameters as well as the dominant contributions from the single-ion anisotropy. For the two-magnon scattering, where the canting effects can be neglected, the theoretical line shapes are found to be in good agreement with experimental data.

The magneto-optical coupling coefficients in NiF_2 are broadly similar to those obtained for CoF_2. This can be seen from Table III, where for completeness we also make comparisons with the other rutile-structure antiferromagnets MnF_2 and FeF_2 that were previously studied.[5] In future work we shall report on more detailed experimental and theoretical investigations of the one-magnon light scattering in CoF_2 and NiF_2 in order to complement the two-magnon studies given here.

ACKNOWLEDGMENTS

This work was partially supported by the Natural Sciences and Engineering Research Council of Canada (NSERC). The authors thank J. Johnson and G. Wilson for assistance in the Raman spectra analysis, G. Chapman for mass measurements, and H. J. Labbé for the sample preparation and technical assistance in the NiF_2 Raman measurements.

*eric@physics.mun.ca; Present address: Department of Physics and Physical Oceanography, Memorial University of Newfoundland, St John's, Newfoundland, Canada A1B 3X7.

[1] M. G. Cottam and D. J. Lockwood, *Light Scattering in Magnetic Solids* (Wiley, New York, 1986).
[2] J. Cipriani, S. Racine, and R. Dupeyrat, Phys. Lett. **34A**, 187 (1971).
[3] P. A. Fleury, Phys. Rev. **180**, 591 (1969).
[4] M. T. Hutchings, M. F. Thorpe, R. J. Birgeneau, P. A. Fleury, and H. J. Guggenheim, Phys. Rev. B **2**, 1362 (1970).
[5] D. J. Lockwood and M. G. Cottam, Phys. Rev. B **35**, 1973 (1987).
[6] L. J. Zimring and J. W. Stout, J. Chem. Phys. **51**, 4197 (1969).
[7] R. M. MacFarlane and S. Ushioda, Solid State Commun. **8**, 1081 (1970).
[8] R. M. MacFarlane, Phys. Rev. Lett. **25**, 1454 (1970).
[9] J. T. Hoff, P. A. Grunberg, and J. A. Koningstein, Appl. Phys. Lett. **20**, 358 (1972).
[10] P. Moch, J. P. Gosso, and C. Dugautier, in *Light Scattering in Solids*, edited by M. Balkanski (Flammarion, Paris, 1971), p. 138.
[11] W. J. Brya, P. M. Richards, and P. A. Fleury, AIP Conf. Proc. **10**, 729 (1973).
[12] D. J. Lockwood and Z. R. Wasilewski, Phys. Rev. B **70**, 155202 (2004).
[13] R. A. Cowley and W. J. L. Buyers, Rev. Mod. Phys. **44**, 406 (1972).
[14] R. J. Elliott and M. F. Thorpe, J. Phys. C **2**, 1630 (1969).
[15] S. P. Bayrakci, T. Keller, K. Habicht, and B. Keimer, Science **312**, 1926 (2006).
[16] E. Meloche, M. G. Cottam, V. P. Gnezdilov, and D. J. Lockwood, J. Magn. Magn. Mater. **310**, 1593 (2007).
[17] M. G. Cottam, V. So, D. J. Lockwood, R. S. Katiyar, and H. J. Guggenheim, J. Phys. C **16**, 1741 (1983).
[18] M. E. Lines, Phys. Rev. **137**, A982 (1965).